Research Article | Vol. 14, No. 6 / 1 Jun 2023 / Biomedical Optics Express 2551
Biomedical Optics EXPRESS

Visualizing drug-induced lipid accumulation in lysosomes of live cancer cells with stimulated Raman imaging

YUHAO YUAN,[1,2] EMMANUEL O. OLAWODE,[3,4] L. NATHAN TUMEY,[3] AND FAKE LU[1,*]

[1]Department of Biomedical Engineering, Thomas J. Watson College of Engineering and Applied Science, Binghamton University, State University of New York, Binghamton, NY 13902, USA
[2]Current Address: Department of Electrical and Computer Engineering, Boston University, Boston, MA 02215, USA
[3]School of Pharmacy and Pharmaceutical Sciences, Binghamton University, State University of New York, Binghamton, NY 13902, USA
[4]Current Address: College of Pharmacy, Larkin University, Miami, FL 33169, USA
[*]fakelu@binghamton.edu

Abstract: The low pH of the lysosomal compartment often results in sequestration of chemotherapeutic agents that contain positively charged basic functional groups, leading to anti-cancer drug resistance. To visualize drug localization in lysosomes and its influence on lysosomal functions, we synthesize a group of drug-like compounds that contain both a basic functional group and a bisarylbutadiyne (BADY) group as a Raman probe. With quantitative stimulated Raman scattering (SRS) imaging, we validate that the synthesized lysosomotropic (LT) drug analogs show high lysosomal affinity, which can also serve as a photostable lysosome tracker. We find that long-term retention of the LT compounds in lysosomes leads to the increased amount and colocalization of both lipid droplets (LDs) and lysosomes in SKOV3 cells. With hyperspectral SRS imaging, further studies find that the LDs stuck in lysosomes are more saturated than the LDs staying out of the lysosomes, indicating impaired lysosomal lipid metabolism by the LT compounds. These results demonstrate that SRS imaging of the alkyne-based probes is a promising approach to characterizing the lysosomal sequestration of drugs and its influence on cell functions.

1. Introduction

The design of small-molecule drugs requires a careful balance between hydrophobicity and hydrophilicity in order to achieve optimal properties of absorption, distribution, metabolism, and excretion (ADME) [1]. Many hydrophobic drug cores are appended with amine groups to obtain increased solubility, thus providing the appropriate distribution coefficient logD for intestinal absorption [2]. Unfortunately, lysosomal drug accumulation is inevitable in many situations, wherein drugs with weakly basic groups are entrapped in the acidic lysosomes by virtue of protonation and concomitant low permeability in a low pH environment [3]. Lysosomes play an important role in catabolism by breaking down and recycling proteins and lipids [4]. Lysosomal sequestration impedes drugs from accessing their intracellular target (such as DNAs) and may also result in drug degradation by lysosomal enzymes [5]. On the other hand, how lysosomal drug sequestration affects the normal functions of lysosomes has not been well characterized [6]. Imaging of the drugs in cells would allow us to measure and optimize the ADME properties [7]. By taking advantage of the intrinsic autofluorescence of some drugs, one can image the drug using fluorescence microscopy [8]. However, not all drugs exhibit autofluorescence. Moreover, long-term imaging by fluorescence with exogenous labeling can be problematic due to issues

#487527 https://doi.org/10.1364/BOE.487527
Journal © 2023 Received 10 Feb 2023; revised 31 Mar 2023; accepted 4 Apr 2023; published 8 May 2023

Biomedical Optics EXPRESS

such as photobleaching and phototoxicity. In contrast to fluorescence imaging, SRS imaging relies on chemical bond vibration, which is free from photobleaching, thus facilitating long-term tracking of the targeted molecules [9].

Previous studies in leukemia cells demonstrated that stimulated Raman scattering (SRS) microscopy was able to image and track label-free, non-fluorescent drug molecules in lysosomes [10]. Notably, SRS imaging is sufficiently fast to capture the dynamics of drug delivery and distribution [11]. Despite the unique advantages of SRS imaging, it is often difficult to find a distinct Raman peak of the lysosomotropic drug molecules against the dominant cellular background signals from native biomolecules. To better study the effect of drug accumulation in lysosomes, a design of drug-like compounds with a distinguishable Raman peak over the cellular background is preferred.. Alkynes have been widely demonstrated as a Raman probe with a distinct Raman band in the "silent region" with a peak at ~2220 cm^{-1}, in which native biomolecules show no Raman/SRS signals [12,13]. However, the Raman cross-section of a single alkyne group (C≡C) may not be large enough for some applications. It has been reported that the bisaryl alkyne and bisarylbutadiyne (BADY) group exhibits 4.2- and 27 times higher Raman signal intensity, respectively, compared to a single alkyne bond [14]. Nevertheless, both probes exhibit a clear peak at ~2220 cm^{-1} in the silent region and are highly lipophilic, thus enabling efficient membrane permeability [15]. The BADY probe has been used for imaging mitochondria and lysosomes in live cells with an enhanced signal level and reduced cellular background [16,17].

In this study, to visualize the internalization and influence of lysosomal drugs in live cancer cells, we designed and synthesized a group of drug-like lysosomotropic (LT) compounds containing a BADY probe tethered to various weakly basic functional groups. We then treated SKOV3 cells with these LT compounds and characterized the cells with SRS imaging. SRS imaging at the Raman shifts 2220 cm^{-1}, 2854 cm^{-1}, and 3015 cm^{-1} were used to visualize the LT compounds sequestrated in lysosomes, lipid droplets (LDs containing the CH_2 bonds), and the unsaturation degree of lipids (fatty acids containing C = C bonds) in the cells, respectively [18]. Hyperspectral SRS imaging of the CH band (2800-3100 cm^{-1}) was used to analyze the lipid composition of the LDs [19]. We also used a commercial fluorescence lysosome tracker (DND-189) for validation experiments. We first observed long-term (24 h) retention of the LT compounds in lysosomes and confirmed that they could be used as a non-fluorescent lysosome tracker with higher stability, a higher signal-to-noise (SNR) ratio, and a lower background compared to commercial fluorescence trackers. We then found that lysosomal sequestration of the LT compounds led to an increased amount of LDs and lysosomes, as well as increased colocalization of the two cellular organelles. Furthermore, hyperspectral SRS imaging data revealed that the LDs that are colocalized with lysosomes exhibit a higher saturation degree compared to normal LDs, indicating the impaired lysosomal functions for degradation of lipids in LDs. This result was validated by inhibiting lipogenesis of new LDs using the diacylglycerol acyltransferase inhibitors (DGATis). These results demonstrated that SRS imaging of alkyne-labeled molecules is a promising tool for studying lysosomal sequestration and its influence on cellular functions.

2. Materials and methods

2.1. Design and synthesis of the lysosomotropic (LT) compounds

The lysosomotropic molecules (LT1-10) were prepared using a simple EDC-promoted amide coupling between a primary amine and the bisaryl alkyne (1) or the bisarylbutadiyne (2) (Fig. 1(a)). The products were purified by preparative HPLC and characterized by HPLC, MS, and NMR prior to testing. The lysosomotropic derivatives (LT1-7) were designed to incorporate various tertiary-amine-containing side chains that would be protonated at lysosomal pH, while the control compounds (LT8-10) were designed to have an uncharged (but hydrophilic) side chain that would not be protonated at lysosomal pH. A 20 mM working stock solution of each analog

Biomedical Optics EXPRESS

was prepared in DMSO. The spontaneous Raman spectra of the compounds (Fig. 1(b)) were acquired using a confocal Raman spectroscopy with 785 nm excitation (inVia confocal Raman microscope, Renishaw). All solution samples were prepared on aluminum foil substrates for Raman measurements.

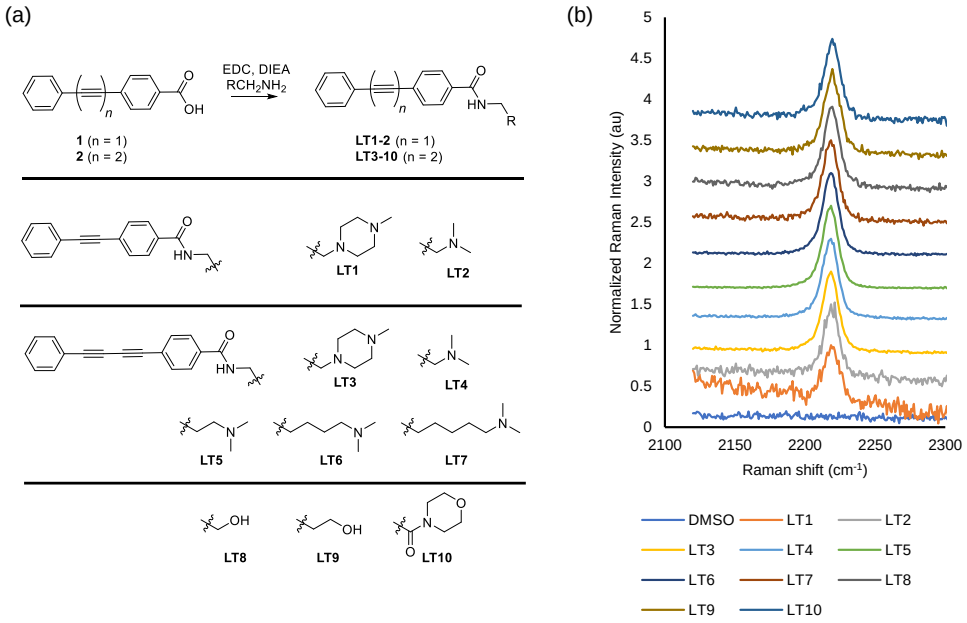

Fig. 1. (a) Chemical structures of the synthesized alkyne-based lysosomotropic (LT) compounds (LT1-7) and non-basic control compounds (LT8-10). (b) The spontaneous Raman spectra of the LT compounds. A characteristic peak of the alkyne bonds was shown at 2220 cm^{-1}.

2.2. Cell culture and treatment

The SKOV3 cell line was a generous gift from Dr. Anthony J. Di Pasqua in the School of Pharmacy and Pharmaceutical Sciences at Binghamton University. Cells were cultured in McCoy's 5A Medium (ATCC) supplemented with 10% Fetal Bovine Serum (ATCC) on cover glasses for 24 hours before treatment. For short-term experiments, cells were treated with 20 μM LT compounds for one hour, the same treatment duration as a commercial lysosome tracker, to examine the lysosomotropic affinity of these compounds. To estimate the long-term effect and retention of the LT compounds, we treated cells with 20 μM LT compounds for 1 hour and then refreshed the media and cultured them for additional 23 hours. Depletion of new LD formation was accomplished by incubating the cells with 20 μM T863 (Sigma-Aldrich) and 10 μM PF-06424439 (Sigma-Aldrich) for 24 hours to inhibit DGAT1 and DGAT2, respectively, and the LD depletion status was maintained during the whole treatment with the presence of DGAT inhibitors (DGATis) [20,21].

2.3. SRS imaging and two-photon fluorescence (TPF) imaging of the cells

The lab-built, integrated stimulated Raman scattering (SRS) and two-photon fluorescence (TPF) microscope was described in detail previously [18]. The pump and Stokes beams were set to an average power of ~145 mW, respectively, before the objective lens. Forward SRS and backward TPF imaging were acquired simultaneously to avoid misalignment between the two

Biomedical Optics EXPRESS

imaging modalities. Live-cell imaging was performed within 20 min after leaving the incubator except for hyperspectral SRS imaging, which used fixed cells with 4% paraformaldehyde (PFA) for 10 min. Live-cell imaging was essential for this study since fixation may compromise the acidity of lysosomes. Hyperspectral SRS imaging of the fixed cells was obtained by changing the wavelength of the pump beam, which eventually covered a range from 2800-3100 cm^{-1} with a step of ~15 cm^{-1} Raman shift. Spectral focusing technology was used to improve the SRS spectral resolution [22]. As control experiments, lysosomes in live SKOV3 cells were labeled with 1 μM the LysoSensor DND-189 (L7535, Invitrogen) for 1 hour and imaged with TPF. TPF imaging of LDs labeled with 2 μM BODIPY (D3922, Invitrogen) for 10 min was used to confirm the SRS contrast of LDs at 2854 cm^{-1}.

2.4. Image processing and statistical analysis

The calculated area ratio of LDs to the cell body was used to evaluate the amount of LDs as described previously [18]. The same method was adopted to quantify the amount of lysosomes. The field of view of all the SRS images was 175 μm by 175 μm with pixels of 1024 by 1024. The area of lysosomes was measured by thresholding the SRS images at 2220 cm^{-1}. The area of the cell body was measured by thresholding the SRS images at 2854 cm^{-1}. More than 4 images were analyzed for each group. The same laser power was used and confirmed each time before the experiments. For each experimental session, imaging data were acquired within a few hours. And the same thresholding parameters were adopted among all groups to minimize potential bias. The SRS spectra were plotted using the hyperspectral SRS imaging data. The spectra of multiple clusters of lipid droplets (LDs) ($n > 7$ from different cells and each cluster had more than 100 pixels) were analyzed for each experimental group for statistical analysis. To quantify the amount of LDs and lysosomes under various treatments, a two-sample t-test and one-way ANOVA analysis were performed in Excel. To quantify the colocalization degree, Pearson's coefficient between 8-bit SRS images at 2220 cm^{-1} and 8-bit TPF images was calculated with JACoP and the Colocalization Finder in ImageJ [23,24]. A two-sample t-test was performed to compare Pearson's coefficient in Excel. $P < 0.05$ was considered statistically significant. All experiments were repeated three times.

3. Results

3.1. SRS imaging of BADY-labeled LT compounds sequestrated in lysosomes

We measured the Raman spectra of the synthesized LT1-10 compounds and found the anticipated characteristic acetylene peak at ~2220 cm^{-1} (Fig. 1) located in the Raman silent region of cells. We first tested the short-term lysosomal sequestration of the LT compounds. The SKOV3 cells were treated with both 1 μM DND-189 (a fluorescence lysosome tracker) and 20 μM LT1-7 compounds for one hour and imaged the cells with SRS and TPF simultaneously (Fig. 2(a)). We found that the LT compounds were able to label the lysosomes, which was validated by colocalization of the SRS signals at 2220 cm^{-1} (the alkyne bonds in BADY) and TPF signals of the DND-189 dye (Fig. 2(b)). Notably, the LT3-7 compounds yielded strong SRS signals with higher contrast and a reduced cellular background compared to the fluorescence tracker, demonstrating that they can be used as a non-fluorescent lysosome tracker. Consistent with the proposed mechanism of "lysosomal trapping," all three non-basic control analogs (LT8-10) did not show specific lysosomotropic accumulation (Fig. S1). We also found that one-hour treatment with the LT compounds did not induce clear changes in cell morphology and viability.

Retaining drugs in lysosomes is a fundamental characteristic of lysosomotropic drug sequestration in which lysosomes may function as a reservoir that minimizes the cytotoxicity of chemotherapeutic agents [3]. To evaluate the long-term (24 h) retention of the LT compounds as lysosomotropic drug analogs, SKOV3 cells were treated with 20 μM of LT4 for one hour,

Biomedical Optics EXPRESS

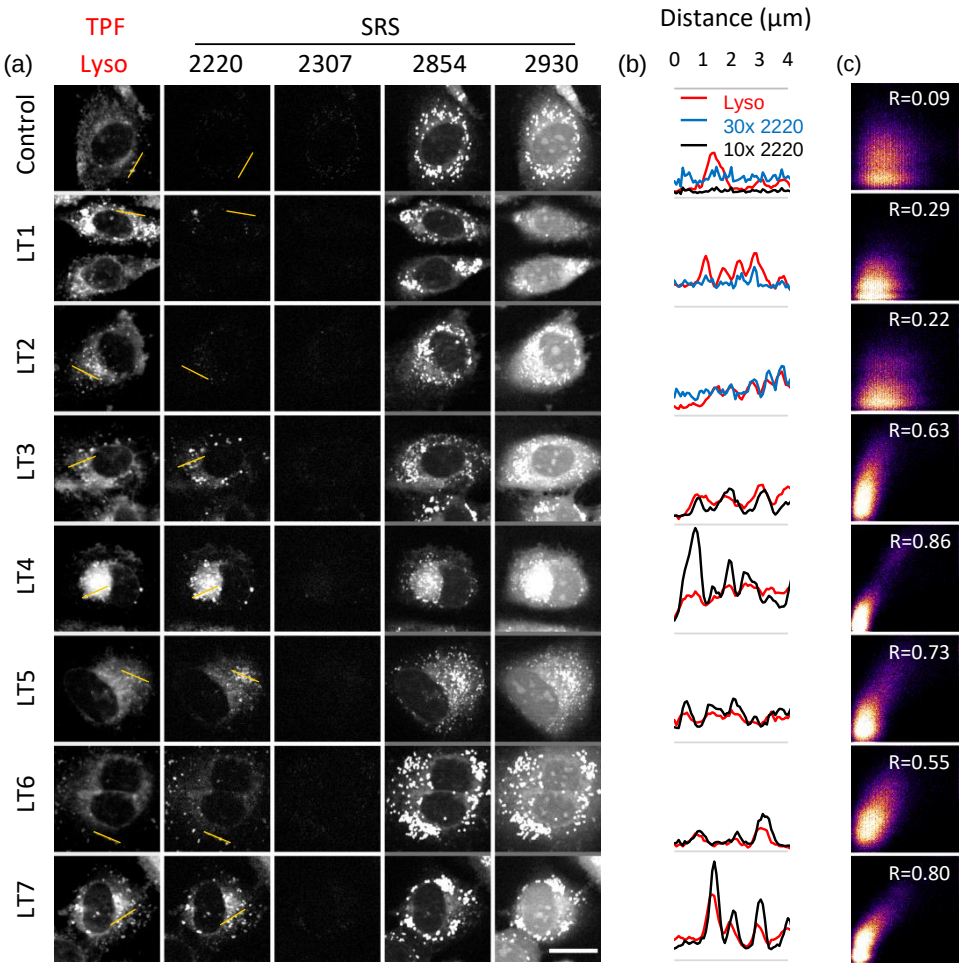

Fig. 2. Short-term (1 h), highly specific lysosomal sequestration of the lysosomotropic compounds (LT3-7) was validated by comparing it to a commercial fluorescence lysosome tracker DND-189. (a) The representative SRS and TPF images of SKOV3 cells treated with 20 μM LTs and 1 μM DND-189 for 1 hour. The Raman peak at 2220 cm-1 was attributed to the alkyne bonds (C≡C), 2307 cm-1 was non-SRS background, 2854 cm-1 was attributed to the CH2 bond representing lipids, and 2930 cm-1 was attributed to the CH3 bond representing proteins. Scale bar, 20 μm. (b) The intensity profiles along the yellow lines shown in (a) reveal the colocalization of the LT compounds (blue/black) and DND-189 (red) labeling lysosomes. (c) The scatter plots of TPF and SRS signals at 2220 cm-1 in (a), with the corresponding Pearson's coefficients R.

Biomedical Optics EXPRESS

followed by regular culture using fresh media for an additional 22 h. Then lysosomes in live cells were labeled with the DND-189 dye for one hour before conducting SRS/TPF imaging (Fig. 3(a)). As shown in Fig. 3(b), we observed faithful retention of LT4 in lysosomes up to 24 h. Compared to fluorescence imaging, SRS imaging of the LT4 compound based on the 2220 cm^{-1} peak exhibited a much lower cellular background, indicating a high affinity of LT4 with lysosomes. The scatter plot of the TPF and SRS signals shows substantial colocalization of LT4 and DND-189 in lysosomes with an R-value of 0.76. Based on these results, we conclude that our BADY-labeled LT compounds could be used as drug analogs to study lysosomal drug sequestration. Meanwhile, they can also be used as a highly sensitive, non-fluorescent Raman/SRS lysosome tracker. Previous studies also reported similar molecular designs with different Raman probes combined with basic groups, which could serve as Raman lysosome trackers [15,17].

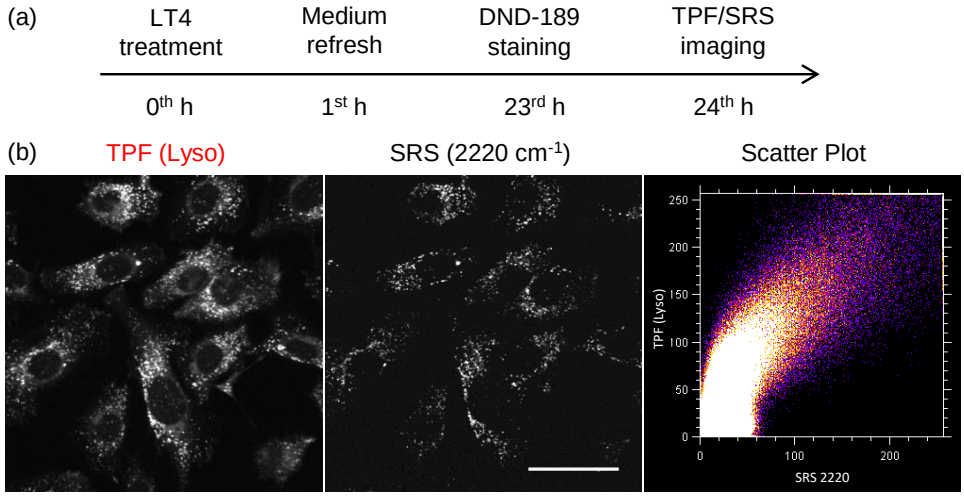

Fig. 3. (a) Protocol of cell treatment to evaluate long-term (24 h) LT4 retention in lysosomes of SKOV3 cells. (b) Left: TPF image of the lysosome tracker DND-189; Middle: SRS image of LT4 at 2220 cm^{-1}; Right: Scatter plot of SRS and TPF signals shows substantial colocalization of DND-189 and LT4 in lysosomes with a Pearson's coefficient of R = 0.76. Scale bar, 50 μm.

3.2. *Sequestration of the LT compounds in lysosomes led to LDs accumulation*

How does lysosomal sequestration of the LT compounds affect the functions of the cancer cells? To address this question, we examined the cells with SRS imaging. Surprisingly, SRS imaging at 2854 cm^{-1} (CH_2) revealed that long-term (24 h) retention of the LT4 compound in lysosomes led to increased LD amount (Fig. 4(a)). SRS imaging of the LDs was validated by TPF imaging with BODIPY staining, a neutral lipid dye (Fig. S2) [18]. Compared to untreated cells, LT4-treated cells contained 1.8-fold more LDs (Fig. 4(b)). In contrast, we did not see increased LDs content in the cells treated with DND-189. These results indicate that long-term sequestration of the lysosomotropic drug analogs affected the normal functions of the cancer cells. While this study revealed the abnormal lipid metabolic activities in the lysosomes of the cells, there might be other consequences that have not been observed.

To assess the dose-dependent LDs accumulation, we tested the LT compounds at 0, 5, 10, 20, 50, and 100 μM following the same procedure in Fig. 3(a). We observed a positive linear correlation between the LD content and LT compounds concentration (Figs. 5(a), (c)), while the non-basic control compounds did not result in increased lipid accumulation (Figs. 5(b), (c)), even with 24-hour long-term treatment (Fig. S3). In addition, high contrast imaging of the LT4

Biomedical Optics EXPRESS

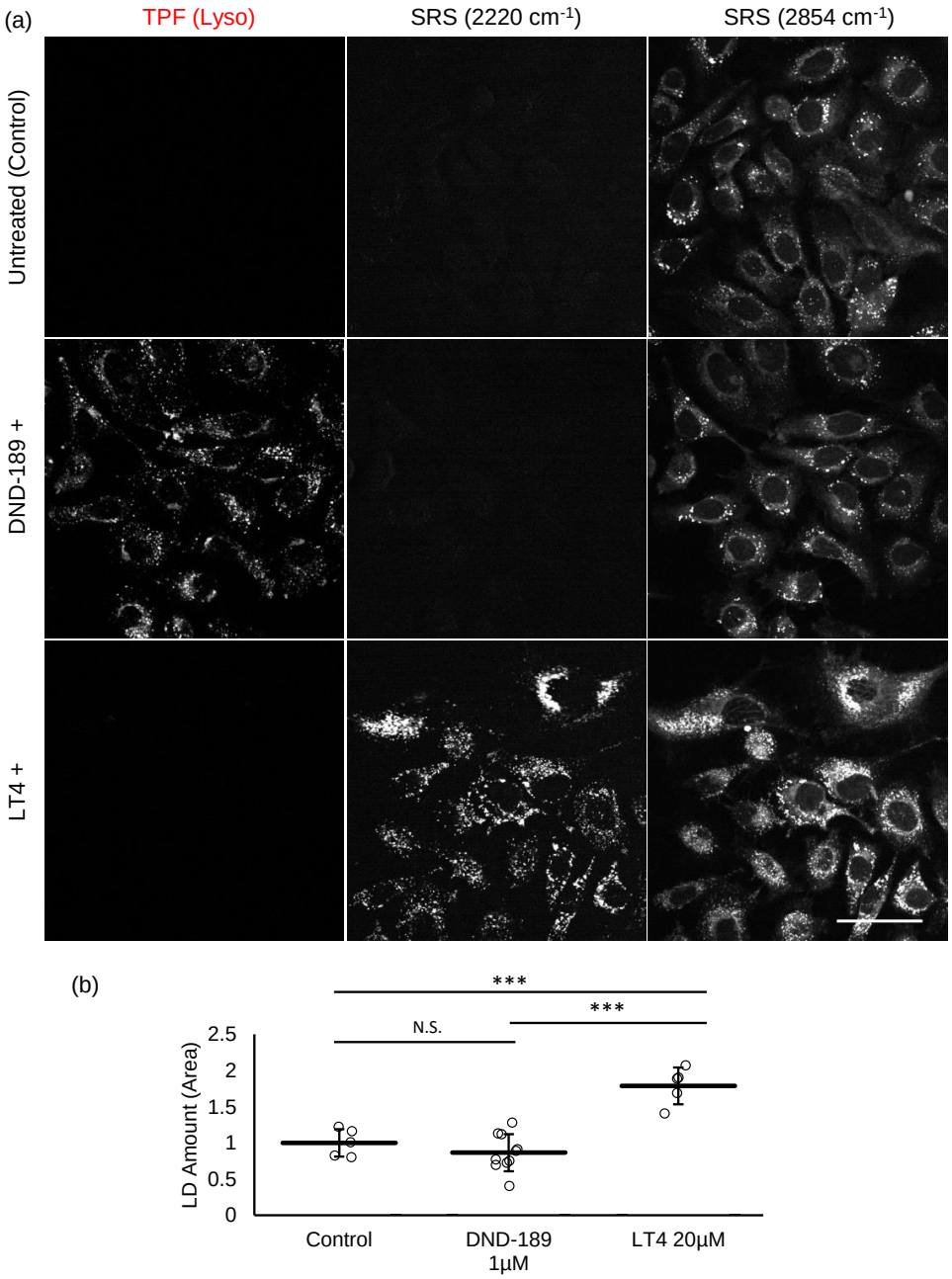

Fig. 4. Long-term (24 h) retention of LT4 in lysosomes led to increased LDs content in SKOV3 cells. (a) The first row: untreated cells (control); the second row: cells treated with 1 μM DND-189 for 1 h; and the third row: cells treated with 20 μM LT4 for 1 h, followed by normal culture with fresh media for 23 h before imaging. All cells were imaged with TPF (column-1), and SRS at Raman shifts 2220 cm^{-1} (C≡C) (column-2), and 2854 cm^{-1} (CH_2) (column-3), respectively. Scale bar, 50 μm. (b) Quantification of LDs measured by SRS images at 2854 cm^{-1}. A two-sample t-test was performed. N.S., not significant; ***$P < 0.001$.

Biomedical Optics EXPRESS

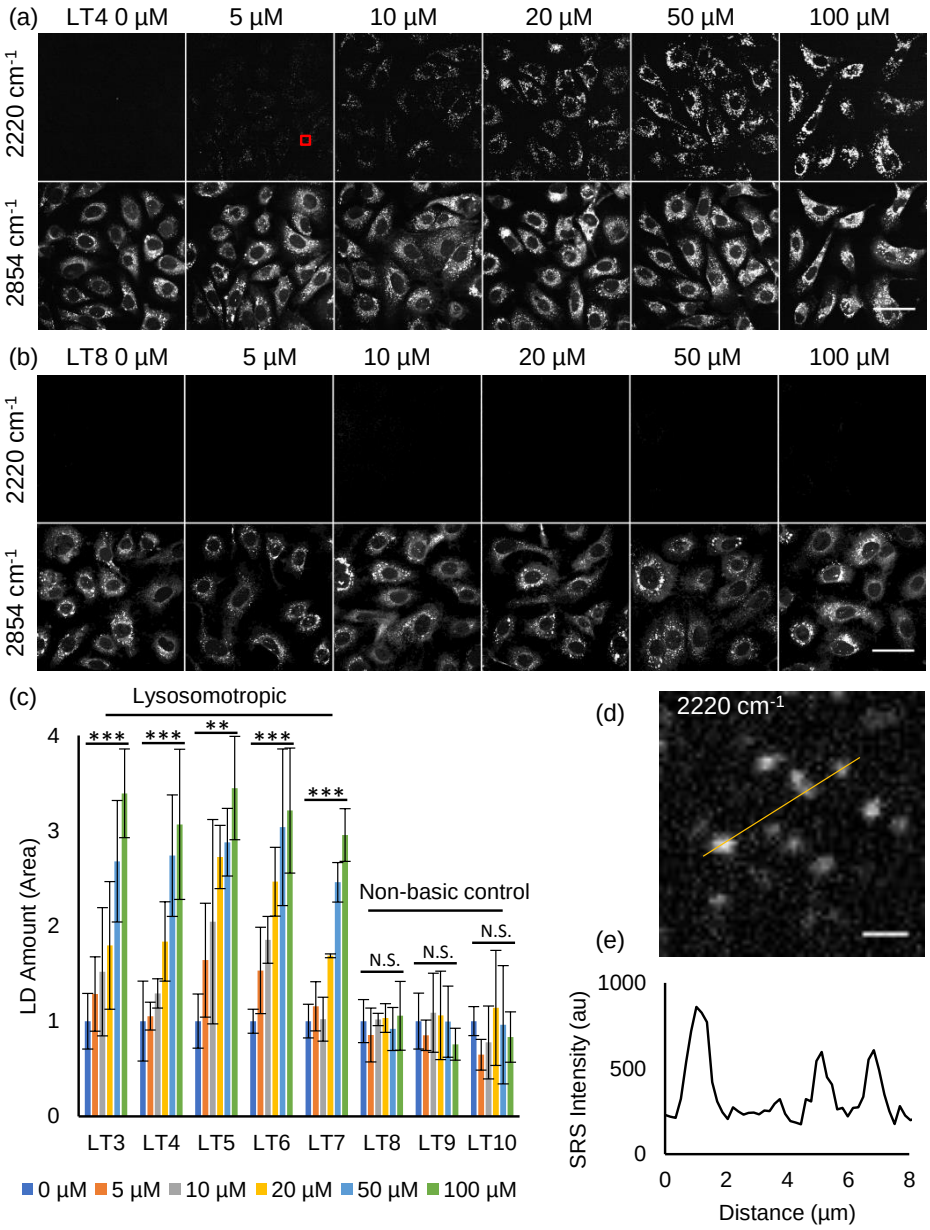

Fig. 5. Long-term (24 h) retention of the LT compounds in lysosomes led to increased LDs amount in SKOV3 cells in a dose-dependent manner. Cells were treated with LT3-10 for 1 h, then cultured in fresh media for an additional 23 h. (a) Representative SRS images of SKOV3 cells treated with LT4 at increased doses, leading to increased SRS signals at both Raman shifts 2220 cm^{-1} (C≡C) and 2854 cm^{-1} (lipids). (b) Representative SRS images of SKOV3 cells treated with LT8 at increased doses. The treatment did not lead to increased SRS signals at 2854 cm^{-1} (lipids). Images at 2220 cm^{-1} were blank because the non-basic control compound LT8 does not accumulate in cells. Scale bar, 50 μm. (c) Quantification of LDs content treated with LT3-10. The lysosomotropic compounds LT3-7 increased LDs dose-dependently, while the non-basic control compounds LT8-10 did not. Single-factor or one-way ANOVA was performed. N.S., not significant; **P < 0.01; ***P < 0.001. (d) The zoom-in image within the red box in (a, treated with 5 μM LT4) shows high-contrast and high-resolution imaging of single lysosomes with SRS signals at 2220 cm^{-1}. Scale bar, 2 μm. (e) The intensity profile along the yellow line in (d) shows a high signal-to-noise (SNR) ratio for these images.

Biomedical Optics EXPRESS

compound sequestrated in lysosomes with a lower concentration treatment (5 μM) was achieved (Figs. 5(d), (e)).

3.3. Sequestration of the LT compounds in lysosomes led to increased lysosome amount and increased colocalization of LDs and lysosomes

After we observed the increased LD content induced by the sequestration of the LT compounds in lysosomes, we sought to understand the interaction between LDs and lysosomes. Lysosomes play an important role in lipid catabolism and transport, which is a critical step in cellular lipid metabolism [25]. In our experiments, we found that cells treated with LT4 for 24 h contained higher content of both LDs (SRS, pseudo-color green) and lysosomes (TPF, red), as shown in Figs. 6(a), (b). Quantitative analysis with Pearson's coefficient confirms that cells treated with LT4 had increased colocalization of LDs and lysosomes compared to the untreated cells (Figs. 6(a), (c)). The increased amount of lysosomes was indicated by the 2.57-fold stronger TPF signals of the lysosome tracker DN-189 dye in the LT4-treated cells compared to the untreated cells (Fig. 6(b)), which may be explained by the compensatory mechanism of lysosome biogenesis in health and disease [26]. We speculate that our lysosomotropic compounds impeded the fundamental functions of lysosomes, which perhaps prevented lipid degradation and therefore resulted in lipids accumulation in the lysosomal lumen. Further evidence is required to verify this observation.

3.4. Sequestration of the LT4 compound led to increased lipid saturation of the LDs stuck in lysosomes

To further investigate the altered biogenesis of the LDs associated with lysosomes, we stopped new LD formation using the diacylglycerol acyltransferase inhibitors (DGATis), 20 μM T863, and 10 μM PF-06424439, prior to the LT4 treatment [18,27]. The inhibitors resulted in a nearly complete depletion of LDs (0.18-fold of the control) in cultured SKOV3 cells (Fig. 7(a), the first and third columns, and Fig. 7(b)). In contrast, with co-treatment of LT4 and DGATis, a modest amount of LDs (0.65-fold of the control) was still observed (Fig. 7(a), the first and fourth columns, and Fig. 7(b)). In addition, we found that co-treatment of LT4 and DGATis of the cells led to increased colocalization (yellow, which is an overlay of red and green colors) of lysosomes (red) and LDs (green) reflected by the increased Pearson's coefficients (Figs. 7(a), (c)). These results revealed that the sequestration of LT4 in lysosomes disturbed the normal process of lipid degradation in lysosomes.

We further conducted hyperspectral SRS imaging of the cells and measured the SRS spectra (2800-3100 cm^{-1}) of the LDs and surprisingly found that the LDs in LT4-treated cells could be classified into two distinct categories, referred to as type-I and type-II LDs. Type-I LDs exhibited a similar spectral profile to the control LDs in the untreated cells, and they were not colocalized with the lysosomes (Figs. 7(a), the second column; Figs. 7(d),(e)). In particular, type-I LDs showed a clear unsaturation degree characterized by the Raman peak at 3015 cm^{-1} (attributed to the =CH bond) relative to the peak at 2854 cm^{-1} (CH_2) (Fig. S4) [28]. In contrast, type-II LDs were largely colocalized with the lysosomes, indicated by the yellow color in the overlay images (Fig. 7(a), the second and fourth columns). Type-II LDs did not show a clear 3015 cm^{-1} peak, indicating that type-II LDs were more saturated than type-I LDs (Figs 7(f), (g)). Based on these results, we conclude that the dysfunctional lysosomes induced by the sequestration of LT4 led to the accumulation of LDs in lysosomes, and these LDs (type-II) exhibited an abnormally increased saturation degree.

Biomedical Optics EXPRESS

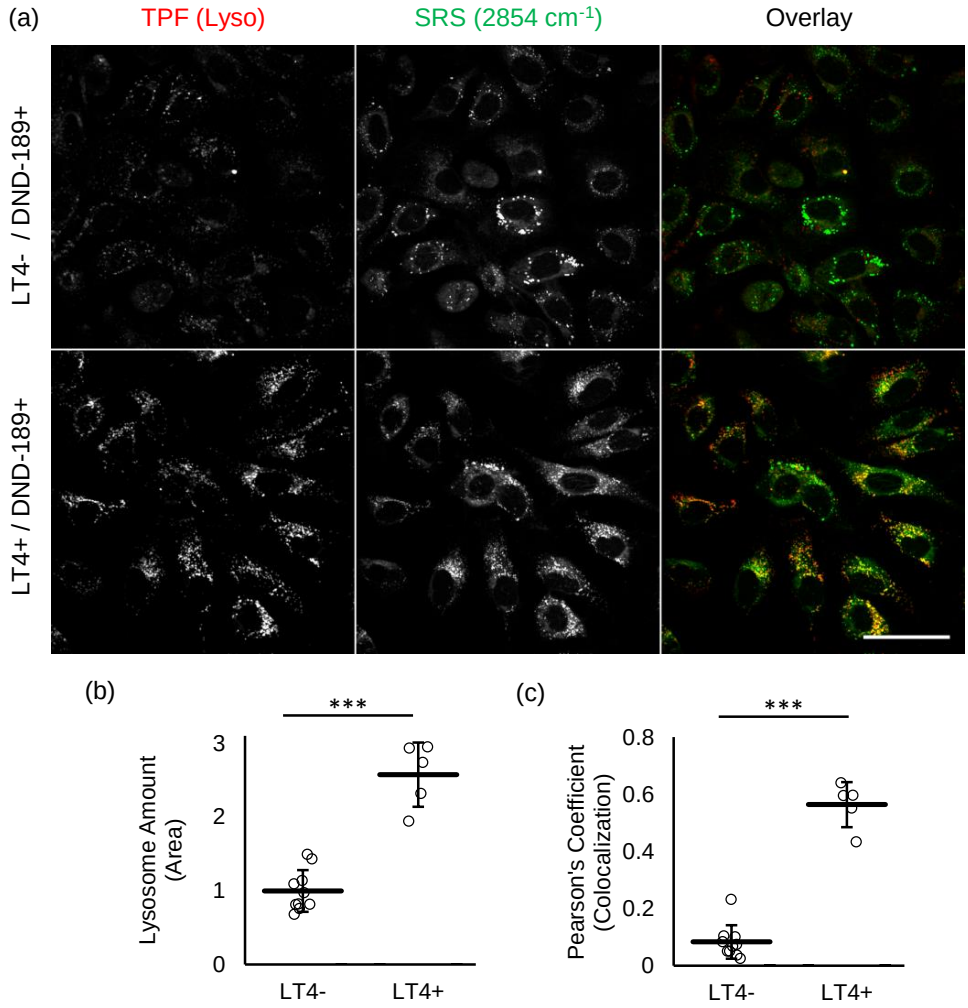

Fig. 6. Long-term (24 h) retention of LT4 in lysosomes led to increased LDs amount and lysosomes amount, as well as their colocalization. (a) The first row: cells were treated with 1 μM DND-189 for 1 h; the second row: cells were treated with 1 μM DND-189 and 20 μM LT4 for 1 h, both followed by normal culture with fresh media for additional 23 h before imaging. Cells were imaged with TPF (lysosomes in pseudo color red) and SRS at Raman shift 2854 cm^{-1} (lipids in green). Scale bar, 50 μm. (b) Increased amount of lysosomes indicated by the increased TPF signals of DND-189. (c) Increased colocalization (yellow) of lysosomes (red) and LDs (green) indicated by the significantly increased Pearson's coefficients. A two-sample t-test was performed. ***$P < 0.001$.

Biomedical Optics EXPRESS

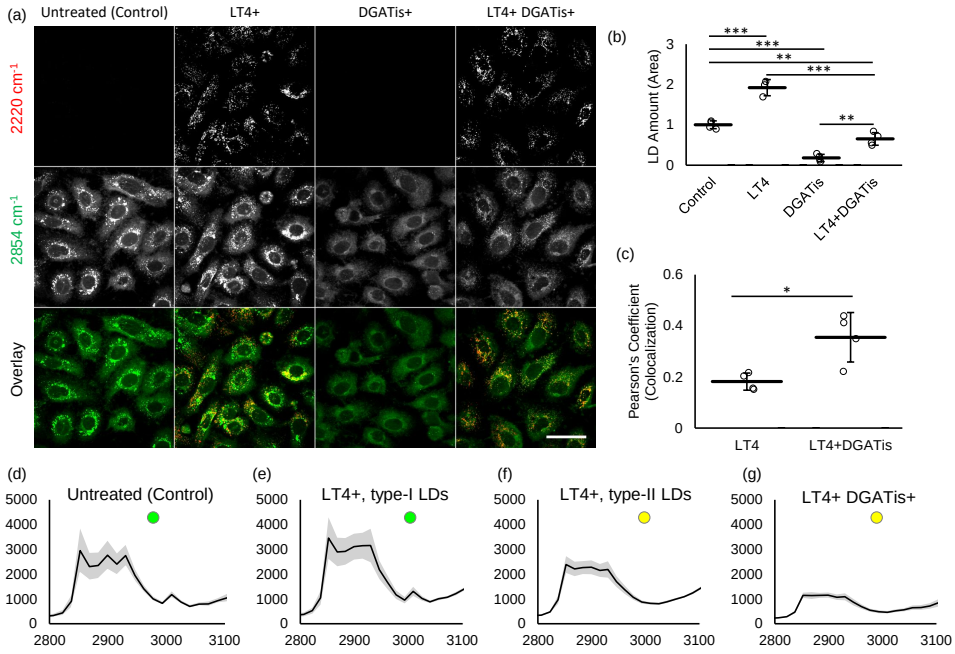

Fig. 7. Two distinct types of LDs (namely type-I and type-II) were found in SKOV3 cells with long-term (24 h) retention of LT4 compound. (a) Cells were treated with or without DGATis from 0^{th} to 48^{th} h and with or without 20 μM LT4 from 24^{th} to 25^{th} h. The first column: untreated cells; the second column: cells treated with LT4; the third column: cells treated with DGATis; and the fourth column: cells co-treated with LT4 and DGATis. Cells were imaged at Raman shifts of 2220 cm^{-1} (C≡C, red) and 2854 cm^{-1} (lipids, green). Scale bar, 50 μm. (b) Quantification of LDs indicated that LT4 led to increased LDs while DGATis depleted LDs. (c) Pearson's coefficients indicated a significantly increased colocalization (yellow) of lysosomes (red) and LDs (green) in cells co-treated with LT4 and DGATis compared to cells treated with LT4 alone. A two-sample t-test was performed. *$P < 0.05$; **$P < 0.01$; ***$P < 0.001$. (d-g) Averaged SRS spectra of LDs in the CH band (2800-3100 cm^{-1}) in cells that were untreated (d), treated with LT4 (e, type-I LDs; f, type-II LDs), and co-treated with LT4 and DGATis (g), respectively.

4. Discussion

Small-molecule drugs with basic groups tend to accumulate in lysosomes, sometimes leading to drug resistance [3]. The acidity of lysosome "traps" lipophilic compounds that contain basic functional groups, which are frequently found on chemotherapeutic agents such as Doxorubicin, Nintedanib, Topotecan, and Imatinib, leading to a reduced drug effect and increased drug dose [8,10,29–31]. In order to better understand lysosomal sequestration of drugs, it is necessary to visualize their uptake and retention in lysosomal compartments. Fluorescence labeling on small drug molecules is less practical due to the dramatic changes in its chemical properties. Therefore, we chose to develop lysosomotropic drug-like compounds with distinguishable optical identification, enabling them to be imaged directly. While some drugs can be imaged based on their autofluorescence, such imaging often suffers from a broad cellular background with photobleaching issues. Here we demonstrated the use of Raman probes as an alternative visualizing tool for microscopic imaging, which overcomes the photobleaching issue in fluorescence [9]. Based on the acidic environment of the lysosomes, our synthesized compounds containing

Biomedical Optics EXPRESS

a weakly basic group and a bright Raman probe exhibited high organelle-specific binding to lysosomes and a high SRS signal level.

In this work, we synthesized a group of Raman-tagged lysosomotropic compounds and used them to observe the process of lysosomal sequestration in live cancer cells. The BADY probe offered very bright Raman and SRS signals, and the weakly basic functional groups showed high affinity to lysosomes. With long-term treatment (24 h), we demonstrated that these compounds could be used as lysosomotropic drug analogs for lysosomal sequestration studies. We found that sequestration and long-term retention of the LT compounds in lysosomes affected the normal functions of the lysosomes. Treatment of the cells with the LT compounds led to increased amounts of both LDs and lysosomes, as well as their colocalization. In particular, the LDs that stuck in the impaired lysosomes exhibited an increased saturation degree level compared to the normal LDs. The increased LD content and changed LD chemical composition were indicators of the impaired lysosomal functions caused by the "toxicity" of the LT compounds. These results demonstrated that the sequestration of small molecule drugs would reduce not only the efficacy of the drug but also affect the normal functions of the cells.

We observed the impaired lysosome functions in terms of lysosomal lipid degradation induced by the LT compounds. These results are consistent with the previous studies [32,33]. The current study was not sought to address the mechanism of lysosomal drug sequestration. Lysosomes contain various enzymes for the degradation of protein, lipids, and polysaccharides, among which an enzyme called lysosomal acid lipase (LAL) is responsible for lipid degradation [34]. It is reasonable to speculate that the LT compounds impeded the normal functions of the LAL enzyme and therefore influenced the LDs digestion in the impaired lysosomes [35]. The change of saturated/unsaturated lipids ratio requires further exploration [36]. With short-term treatment, we validated that these LT compounds can be used as a good Raman-based lysosome tracker. Compared to fluorescent trackers, such as DND-189, the LT compounds exhibited higher specificity staining the lysosomes with a lower cellular background. However, our results also revealed that these Raman-tagged LT compounds induced impaired lysosomal functions for lipid degradation, which limits their applications as a tracker for long-term lysosome imaging studies. Interestingly, we observed a linear correlation between increased LDs and drug dose. In this regard, if a brighter Raman probe is designed and adopted, the concentration and, therefore, the toxicity of the LT compounds may be reduced.

While fluorescence microscopy with chemical staining is routinely used to image neutral lipids in cells, it cannot measure the chemical composition of the lipids. SRS microscopy not only provides high-resolution morphological imaging of the microscale lipid droplets but also probes the chemical composition, as demonstrated in this work and previously [18]. SRS signals are linearly proportional to the concentration of the selected chemical bonds, allowing straightforward quantitative analysis. In addition, unmixing of the SRS spectral data allows the decomposition of various fatty acid species in lipids [18]. The use of Raman tags further increases the SRS imaging contrast with a reduced cellular or tissue background.

5. Conclusion

In this work, we studied the internalization of lysosomotropic compounds and their influence on lysosomal metabolism. We demonstrated that our analogs are entrapped in lysosomes and function as Raman lysosome trackers, performing equivalently or even better than fluorescent trackers in short-term assays. However, we also observed unwanted long-term impairment of lysosomes wherein lipids accumulated in the lysosomal lumen in a dose-dependent manner. Lower drug concentration may reduce this unwanted effect but may diminish the signal-to-noise ratio. Importantly, we could directly see the lysosomotropic drugs with SRS to study lysosomal drug resistance. The compensation by the increased number of lysosomes after lysosomotropic drug sequestration may further enhance the drug resistance of cancer cells. We hypothesize

Biomedical Optics EXPRESS

that suppressing the biogenesis of lysosomes and lysosome-related autophagy or introducing drug-induced lysosomal storage disorder in cancer cells may result in novel approaches for cancer therapy [37,38].

Funding. National Institutes of Health (R01GM140026, R15GM140444).

Acknowledgments. We thank Dr. Anthony J. Di Pasqua for sharing the SKOV3 cell line. We thank Dr. Kenneth Chiu for the helpful discussion of image processing. FL and NT designed the study. EO synthesized the lysosomotropic compounds with the Raman/SRS probe. YY conducted the experiments, analyzed the data, and wrote the manuscript draft. All authors edited the manuscript. We acknowledge funding support from the National Institutes of Health and the Transdisciplinary Areas of Excellence (TAE) Seed Grant at Binghamton University.

Disclosures. The authors declare no conflicts of interest.

Data availability. Data underlying the results presented in this paper are not publicly available at this time but may be obtained from the authors upon reasonable request.

Supplemental document. See Supplement 1 for supporting content.

References

1. L. Di and E. Kerns, *Drug-like Properties: Concepts, Structure Design and Methods from ADME to Toxicity Optimization* (Academic Press, 2015).
2. C. A. M. Hogben, D. J. Tocco, B. B. Brodie, and L. S. Schanker, "On the mechanism of intestinal absorption of drugs," J. Pharmacol. Exp. Ther. **125**, 275 (1959).
3. A. M. Kaufmann and J. P. Krise, "Lysosomal sequestration of amine-containing drugs: analysis and therapeutic implications," J. Pharm. Sci. **96**(4), 729–746 (2007).
4. P. Saftig and J. Klumperman, "Lysosome biogenesis and lysosomal membrane proteins: trafficking meets function," Nat. Rev. Mol. Cell Biol. **10**(9), 623–635 (2009).
5. B. Zhitomirsky and Y. G. Assaraf, "Lysosomal sequestration of hydrophobic weak base chemotherapeutics triggers lysosomal biogenesis and lysosome-dependent cancer multidrug resistance," OncoTargets Ther. **6**(2), 1143–1156 (2015).
6. S. Lu, T. Sung, N. Lin, R. T. Abraham, and B. A. Jessen, "Lysosomal adaptation: How cells respond to lysosomotropic compounds," PLoS One **12**(3), e0173771 (2017).
7. L. M. Kaminskas, B. J. Boyd, and C. J. Porter, "Dendrimer pharmacokinetics: the effect of size, structure and surface characteristics on ADME properties," Nanomedicine **6**(6), 1063–1084 (2011).
8. B. Englinger, S. Kallus, J. Senkiv, D. Heilos, L. Gabler, S. van Schoonhoven, A. Terenzi, P. Moser, C. Pirker, G. Timelthaler, W. Jäger, C. R. Kowol, P. Heffeter, M. Grusch, and W. Berger, "Intrinsic fluorescence of the clinically approved multikinase inhibitor nintedanib reveals lysosomal sequestration as resistance mechanism in FGFR-driven lung cancer," J. Exp. Clin. Cancer Res. **36**(1), 122 (2017).
9. H. J. Lee, W. Zhang, D. Zhang, Y. Yang, B. Liu, E. L. Barker, K. K. Buhman, L. V. Slipchenko, M. Dai, and J.-X. Cheng, "Assessing cholesterol storage in live cells and c. elegans by stimulated Raman scattering imaging of phenyl-diyne cholesterol," Sci. Rep. **5**(1), 7930 (2015).
10. D. Fu, J. Zhou, W. S. Zhu, P. W. Manley, Y. K. Wang, T. Hood, A. Wylie, and X. S. Xie, "Imaging the intracellular distribution of tyrosine kinase inhibitors in living cells with quantitative hyperspectral stimulated Raman scattering," Nat. Chem. **6**(7), 614–622 (2014).
11. B. G. Saar, C. W. Freudiger, J. Reichman, C. M. Stanley, G. R. Holtom, and X. S. Xie, "Video-rate molecular imaging in vivo with stimulated Raman scattering," Science **330**(6009), 1368–1370 (2010).
12. L. Wei, F. Hu, Y. Shen, Z. Chen, Y. Yu, C.-C. Lin, M. C. Wang, and W. Min, "Live-cell imaging of alkyne-tagged small biomolecules by stimulated Raman scattering," Nat. Methods **11**(4), 410–412 (2014).
13. S. Hong, T. Chen, Y. Zhu, A. Li, Y. Huang, and X. Chen, "Live-cell stimulated Raman scattering imaging of alkyne-tagged biomolecules," Angew. Chem., Int. Ed. **53**(23), 5827–5831 (2014).
14. H. Yamakoshi, K. Dodo, A. Palonpon, J. Ando, K. Fujita, S. Kawata, and M. Sodeoka, "Alkyne-tag Raman imaging for visualization of mobile small molecules in live cells," J. Am. Chem. Soc. **134**(51), 20681–20689 (2012).
15. F. Hu, C. Zeng, R. Long, Y. Miao, L. Wei, Q. Xu, and W. Min, "Supermultiplexed optical imaging and barcoding with engineered polyynes," Nat. Methods **15**(3), 194–200 (2018).
16. H. Yamakoshi, A. Palonpon, K. Dodo, J. Ando, S. Kawata, K. Fujita, and M. Sodeoka, "A sensitive and specific Raman probe based on bisarylbutadiyne for live cell imaging of mitochondria," Bioorg. Med. Chem. Lett. **25**(3), 664–667 (2015).
17. C. Ding, Y. Chen, H. Li, B. Wang, Q. Wei, H. Tang, S. Jia, Z. He, P. Wang, and X. Zhou, "Photostable lysosomal imaging of living cell with hyperspectral stimulated Raman scattering microscopy using a probe based on bisarylbutadiyne," Chin. Chem. Lett. **30**(7), 1393–1396 (2019).
18. Y. Yuan, N. Shah, M. I. Almohaisin, S. Saha, and F. Lu, "Assessing fatty acid-induced lipotoxicity and its therapeutic potential in glioblastoma using stimulated Raman microscopy," Sci. Rep. **11**(1), 7422 (2021).
19. S. Yan, S. Cui, K. Ke, B. Zhao, X. Liu, S. Yue, and P. Wang, "Hyperspectral stimulated raman scattering microscopy unravels aberrant accumulation of saturated fat in human liver cancer," Anal. Chem. **90**(11), 6362–6366 (2018).

Biomedical Optics EXPRESS

20. J. Cao, Y. Zhou, H. Peng, X. Huang, S. Stahler, V. Suri, A. Qadri, T. Gareski, J. Jones, S. Hahm, M. Perreault, J. McKew, M. Shi, X. Xu, J. F. Tobin, and R. E. Gimeno, "Targeting Acyl-CoA:diacylglycerol acyltransferase 1 (DGAT1) with small molecule inhibitors for the treatment of metabolic diseases," J. Biol. Chem. **286**(48), 41838–41851 (2011).
21. C. E. Senkal, M. F. Salama, A. J. Snider, J. J. Allopenna, N. A. Rana, A. Koller, Y. A. Hannun, and L. M. Obeid, "Ceramide Is Metabolized to Acylceramide and Stored in Lipid Droplets," Cell Metab. **25**(3), 686–697 (2017).
22. I. Rocha-Mendoza, W. Langbein, and P. Borri, "Coherent anti-Stokes Raman microspectroscopy using spectral focusing with glass dispersion," Appl. Phys. Lett. **93**(20), 201103 (2008).
23. S. Bolte and F. P. Cordelières, "A guided tour into subcellular colocalization analysis in light microscopy," J. Microsc. **224**(3), 213–232 (2006).
24. C. A. Schneider, W. S. Rasband, and K. W. Eliceiri, "NIH Image to ImageJ: 25 years of image analysis," Nat. Methods **9**(7), 671–675 (2012).
25. A. M. Thelen and R. Zoncu, "Emerging roles for the lysosome in lipid metabolism," Trends Cell Biol. **27**(11), 833–850 (2017).
26. L. Bajaj, P. Lotfi, R. Pal, A. d. Ronza, J. Sharma, and M. Sardiello, "Lysosome biogenesis in health and disease," J. Neurochem. **148**(5), 573–589 (2019).
27. C.-L. E. Yen, S. J. Stone, S. Koliwad, C. Harris, and R. V. Farese Jr., "Thematic review series: glycerolipids. DGAT enzymes and triacylglycerol biosynthesis," J. Lipid Res. **49**(11), 2283–2301 (2008).
28. C. W. Freudiger, W. Min, B. G. Saar, S. Lu, G. R. Holtom, C. He, J. C. Tsai, J. X. Kang, and X. S. Xie, "Label-free biomedical imaging with high sensitivity by stimulated Raman scattering microscopy," Science **322**(5909), 1857–1861 (2008).
29. B. Zhitomirsky and Y. G. Assaraf, "Lysosomes as mediators of drug resistance in cancer," Drug Resist. Updates **24**, 23–33 (2016).
30. K. J. Gotink, H. J. Broxterman, M. Labots, R. R. de Haas, H. Dekker, R. J. Honeywell, M. A. Rudek, L. V. Beerepoot, R. J. Musters, G. Jansen, A. W. Griffioen, Y. G. Assaraf, R. Pili, G. J. Peters, and H. M. W. Verheul, "Lysosomal Sequestration of Sunitinib: A Novel Mechanism of Drug Resistance," Clin. Cancer Res. **17**(23), 7337–7346 (2011).
31. B. Guo, A. Tam, S. A. Santi, and A. M. Parissenti, "Role of autophagy and lysosomal drug sequestration in acquired resistance to doxorubicin in MCF-7 cells," BMC Cancer **16**(1), 762 (2016).
32. S. Schlager, N. Vujic, M. Korbelius, M. Duta-Mare, J. Dorow, C. Leopold, S. Rainer, M. Wegscheider, H. Reicher, U. Ceglarek, W. Sattler, B. Radovic, and D. Kratky, "Lysosomal lipid hydrolysis provides substrates for lipid mediator synthesis in murine macrophages," Oncotarget **8**(25), 40037–40051 (2017).
33. A. S. Rambold, S. Cohen, and J. Lippincott-Schwartz, "Fatty acid trafficking in starved cells: regulation by lipid droplet lipolysis, autophagy, and mitochondrial fusion dynamics," Dev. Cell **32**(6), 678–692 (2015).
34. T. Lübke, P. Lobel, and D. E. Sleat, "Proteomics of the lysosome," Biochim. Biophys. Acta, Mol. Cell Res. **1793**(4), 625–635 (2009).
35. C. Settembre and A. Ballabio, "Lysosome: regulator of lipid degradation pathways," Trends Cell Biol. **24**(12), 743–750 (2014).
36. Y. Mizunoe, M. Kobayashi, R. Tagawa, Y. Nakagawa, H. Shimano, and Y. Higami, "Association between lysosomal dysfunction and obesity-related pathology: a key knowledge to prevent metabolic syndrome," Int. J. Mol. Sci. **20**(15), 3688 (2019).
37. S. Piao and R. K. Amaravadi, "Targeting the lysosome in cancer," Ann. N. Y. Acad. Sci. **1371**(1), 45–54 (2016).
38. F. Geng and D. Guo, "Lipid droplets, potential biomarker and metabolic target in glioblastoma," Intern. Med. Rev. **3**, 18443 (2017).